A dural lymphatic vascular system that drains brain interstitial fluid and macromolecules

Aleksanteri Aspelund,[1,2] Salli Antila,[1,2] Steven T. Proulx,[3] Tine Veronica Karlsen,[4] Sinem Karaman,[3] Michael Detmar,[3] Helge Wiig,[4] and Kari Alitalo[1,2]

[1]Wihuri Research Institute and [2]Translational Cancer Biology Program, Biomedicum Helsinki, University of Helsinki, 00014 Helsinki, Finland
[3]Institute of Pharmaceutical Sciences, Swiss Federal Institute of Technology (ETH Zurich), CH-8093 Zurich, Switzerland
[4]Department of Biomedicine, University of Bergen, 5009 Bergen, Norway

The central nervous system (CNS) is considered an organ devoid of lymphatic vasculature. Yet, part of the cerebrospinal fluid (CSF) drains into the cervical lymph nodes (LNs). The mechanism of CSF entry into the LNs has been unclear. Here we report the surprising finding of a lymphatic vessel network in the dura mater of the mouse brain. We show that dural lymphatic vessels absorb CSF from the adjacent subarachnoid space and brain interstitial fluid (ISF) via the glymphatic system. Dural lymphatic vessels transport fluid into deep cervical LNs (dcLNs) via foramina at the base of the skull. In a transgenic mouse model expressing a VEGF-C/D trap and displaying complete aplasia of the dural lymphatic vessels, macromolecule clearance from the brain was attenuated and transport from the subarachnoid space into dcLNs was abrogated. Surprisingly, brain ISF pressure and water content were unaffected. Overall, these findings indicate that the mechanism of CSF flow into the dcLNs is directly via an adjacent dural lymphatic network, which may be important for the clearance of macromolecules from the brain. Importantly, these results call for a reexamination of the role of the lymphatic system in CNS physiology and disease.

CORRESPONDENCE
Kari Alitalo:
kari.alitalo@helsinki.fi

Abbreviations used: A488-OVA, Alexa Fluor 488–conjugated OVA; CFS, cerebrospinal fluid; CNS, central nervous system; dcLN, deep cervical LN; DiI, 1,1′-dioctadecyl-3,3,3′,3′-tetramethylindocarbocyanine; EC, endothelial cell; IFP, ISF pressure; ISF, interstitial fluid; PEG, poly(ethylene glycol); PFA, paraformaldehyde; RT, room temperature; scLN, superficial cervical LN; TG, transgenic.

Lymphatic circulation extends throughout most of the body and contributes to tissue homeostasis and function by facilitating the clearance of excess fluid and macromolecules from the interstitium (Secker and Harvey, 2015). However, the central nervous system (CNS) is considered to lack lymphatic vasculature, which has raised long-standing questions about how cerebral interstitial fluid (ISF) is cleared of waste products (Iliff and Nedergaard, 2013). The exchange of compounds is limited by the blood–brain barrier, which functions as a diffusion barrier between the brain and circulating blood. Therefore, the transvascular clearance of most compounds is dependent on specific active transporter mechanisms (Zlokovic, 2011). In addition, the brain has adapted to use a unique paravascular route in which fluids may freely exchange between the brain ISF and the cerebrospinal fluid (CSF) along glial "lymphatic" (glymphatic) routes without crossing the tightly regulated endothelial cell (EC) layer (Iliff et al., 2012; Xie et al., 2013). Downstream of the glymphatic system, the majority of the CSF is considered to drain into the venous circulation through arachnoid granulations. Still, several studies have found that a substantial proportion of the CSF is also drained into extracranial lymphatic vessels and LNs (Koh et al., 2005). However, the mechanisms of CSF entry into the extracranial lymphatic compartment are unclear.

The visualization of lymphatic vessels has been markedly facilitated over the last decade by the identification of specific lymphatic EC markers, such as prospero homeobox protein 1 (PROX1) transcription factor, a master regulator in the program specifying the lymphatic EC fate (Hong et al., 2002), vascular endothelial growth factor receptor 3 (VEGFR3), a lymphangiogenic tyrosine kinase receptor (Secker and Harvey, 2015), chemokine (C-C motif) ligand 21 (CCL21), a chemokine secreted by lymphatic ECs which facilitates the migration of dendritic cells into LNs (Liao and von der Weid, 2015), lymphatic vessel endothelial hyaluronan

The Journal of Experimental Medicine

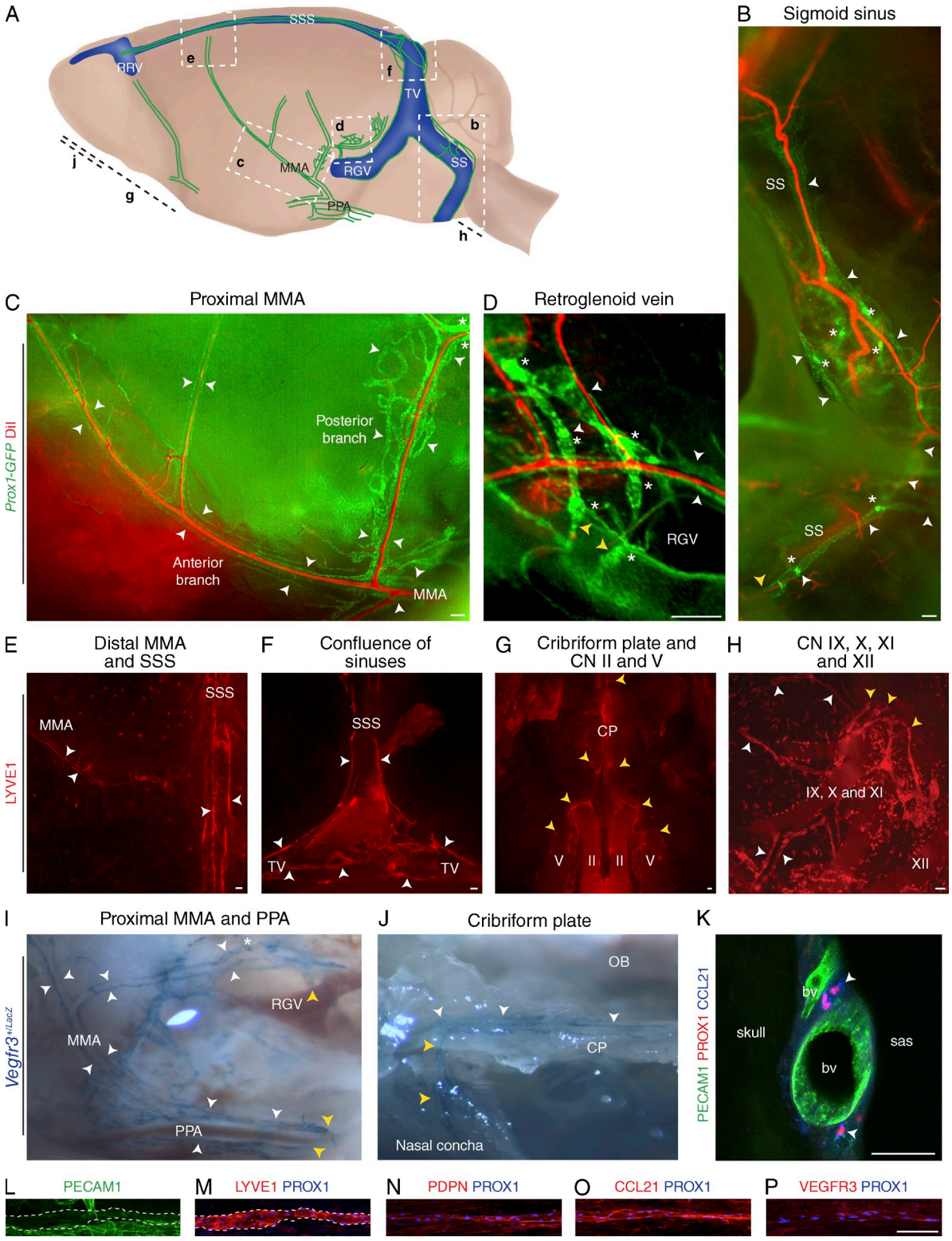

Figure 1. Terminally differentiated lymphatic vessels in the dura mater of the brain. Visualization of CNS lymphatic vasculature using *Prox1-GFP* reporter mice with DiI counterstaining for blood vasculature, *Vegfr3*$^{+/LacZ}$ reporter mice and immunofluorescence for PECAM1, and the lymphatic markers PROX1, LYVE1, PDPN, CCL21, and VEGFR3, as indicated. White arrowheads denote lymphatic vessels, yellow arrowheads denote the skull exit sites, and asterisks denote valves. (A) A schematic image of the various areas analyzed. The letters in bold refer to the corresponding images below. MMA, middle meningeal artery; PPA, pterygopalatine artery; RGV, retroglenoid vein; RRV, rostral rhinal vein; SS, sigmoid sinus; SSS, superior sagittal sinus; TV, transverse vein. (B) Lymphatic vessels running down along the SS and exiting the skull. (C) Lymphatic vessels running down along the proximal MMA branches.

receptor 1 (LYVE1), and podoplanin (PDPN; Oliver and Srinivasan, 2010). We have recently discovered that in the eye, another immune-privileged organ previously considered to lack lymphatic circulation, the Schlemm's canal is a lymphatic-like vessel (Aspelund et al., 2014). These intriguing inconsistencies and our recent discoveries led us to investigate the possibility of lymphatic circulation in the CNS in more detail.

RESULTS AND DISCUSSION

Lymphatic vessels in the dura mater surrounding the brain

The brain is enveloped by meningeal linings consisting of three layers: the pia mater tightly attached to the surface of the brain, the avascular arachnoid mater overlying the subarachnoid space, and the vascularized dura mater fused to the cranial bones. To determine whether lymphatic vessels exist within the CNS and surrounding meninges, we analyzed the *Prox1-GFP* and *Vegfr3*$^{+/LacZ}$ reporter mice and whole-mount immunofluorescence preparations of the skull and brain of WT mice against LYVE1, PROX1, PDPN, CCL21, VEGFR3, and PECAM1. To visualize blood vessels, the *Prox1-GFP* mice were perfused with the fluorescent dye 1,1′-dioctadecyl-3,3,3′,3′-tetramethylindocarbocyanine (DiI; Li et al., 2008).

After removing the brain from the skull, no lymphatic vessels were seen on the brain parenchyma or pia mater (not depicted). However, a surprisingly extensive network of lymphatic vessels was observed in the meninges underlying the skull bones (Fig. 1, A–J; and Video 1). In sagittal planes of the inner skull, lymphatic vessels were observed to run down toward the base of the skull along the transverse sinus, the sigmoid sinus, the retroglenoid vein, the rostral rhinal vein, and the major branches of the middle and anterior meningeal arteries (Fig. 1, B and D; and Video 1). In preparations of the superior portions of the skull, the lymphatic vessels were visualized along the superior sagittal sinus, the transverse sinus, the rostral rhinal veins, and the middle meningeal artery (Fig. 1, E and F). A concentration of lymphatic vessels could be observed to exit the skull along the meningeal portions of the pterygopalatine artery, a branch of the internal carotid artery which dives in and out of the skull to give rise to the middle meningeal artery (Fig. 1 I). Lymphatic vessels along the sigmoid sinus and retroglenoid vein exited the skull along the veins (Fig. 1, B and D). In preparations of the base of the skull, lymphatic vessels could be seen in the distal portion of several cranial nerves (optic, trigeminal, glossopharyngeal, vagus, and accessory), exiting the skull along the nerve (Fig. 1, G and H). Lymphatic vessels could be observed also in the dural lining of the cribriform plate, where some vessels passed through the skull into the nasal mucosa (Fig. 1, G and J).

Generally, lymphatic vessels were relatively scarce in the superior portions of the skull, whereas the base of the skull contained a more extensive lymphatic vessel network (Fig. 1 A). Interestingly, only the lymphatic vessels at the base of the skull contained valves, but their distribution was relatively scarce. Valves were separated by long stretches of valveless vessel segments (Fig. 1, B–D).

To determine the localization of these vessels in relation to the meninges, thick skull sections were analyzed. In these preparations, PROX1- and CCL21-positive lymphatic vessels were observed in the meninges underlying the bony parts of the skull, adjacent to the dural blood vasculature (Fig. 1 K).

Whole-mount immunofluorescence staining of the superior sagittal lymphatic vessels showed that, like conventional lymphatic vessels, the dural lymphatic vessels express very low levels of PECAM1 (Fig. 1 L) but high levels of LYVE1, PDPN, VEGFR3, CCL21, and PROX1 (Fig. 1, M–P; Aspelund et al., 2014). Thus, the dural lymphatic vessels are lined by terminally differentiated lymphatic endothelium.

Overall, these data indicated that lymphatic vessels are present in the dura mater of the CNS and drain out of the skull via the foramina of the base of the skull alongside arteries, veins, and cranial nerves. We named these lymphatic vessels on the basis of their venous, arterial, or cranial nerve counterparts. The localization of the vessels suggested a possible role in CSF absorption through the arachnoid mater.

Dura mater lymphatic vessels drain brain ISF into deep cervical LNs (dcLNs)

Tracers injected into the brain ISF have been shown to translocate into the CSF via the glymphatic system and further into dcLNs (Koh et al., 2005; Iliff et al., 2012; Plog et al., 2015). However, it is unclear how these tracers gain access into the LNs. We hypothesized that the dura mater lymphatic vessels absorb brain ISF and CSF. To test this, we injected an inert 20-kD poly(ethylene glycol) (PEG) conjugate of the bright near-infrared dye IRDye 680 (PEG-IRDye; Proulx et al., 2013) into the brain parenchyma of the *Prox1-GFP* mice. 2 h after injection, the tracer was observed to exit the brain via paravenous routes for entry into the CSF space (not depicted), as previously reported (Iliff et al., 2012). Lymphatic

(D) Lymphatic vessels around the RGV with some vessels exiting the skull. (E–H) Whole-mount LYVE1 immunofluorescence of the skull top and base. (E) Lymphatic vessels along the SSS and the distal parts of the anterior MMA branch extending toward the bregma. (F) Lymphatic vessels along the SSS, bifurcating into the TVs at the confluence of sinuses. (G) Lymphatic vessels exiting the skull along the optic (II) and the trigeminal (V) nerves and through the cribriform plate (CP). CN, cranial nerve. (H) Lymphatic vessels associated with the glossopharyngeal (IX), vagus (X), and accessory (XI) nerves. XII, hypoglossal nerve. (I and J) Stereomicrographs of tissues in a *Vegfr3*$^{+/LacZ}$ reporter mouse showing the skull exit of dural lymphatic vessels along the PPA (I) and through the CP into a nasal concha. OB, olfactory bulb area. (K) Immunofluorescence of thick skull section for PECAM1, PROX1, and CCL21. bv, blood vessel; sas, subarachnoid space. (L–P) Whole-mount immunofluorescence staining of superior sagittal lymphatic vessels with antibodies against PECAM1 (L), LYVE1 (M), PDPN (N), CCL21 (O), VEGFR3 (P), and PROX1 (M–P). LYVE1 and PECAM1 colocalization is indicated with the dashed lines. n = 2–3 per staining. Data are from two to three independent experiments. Bars: (B–H and L–P) 100 µm; (K) 50 µm.

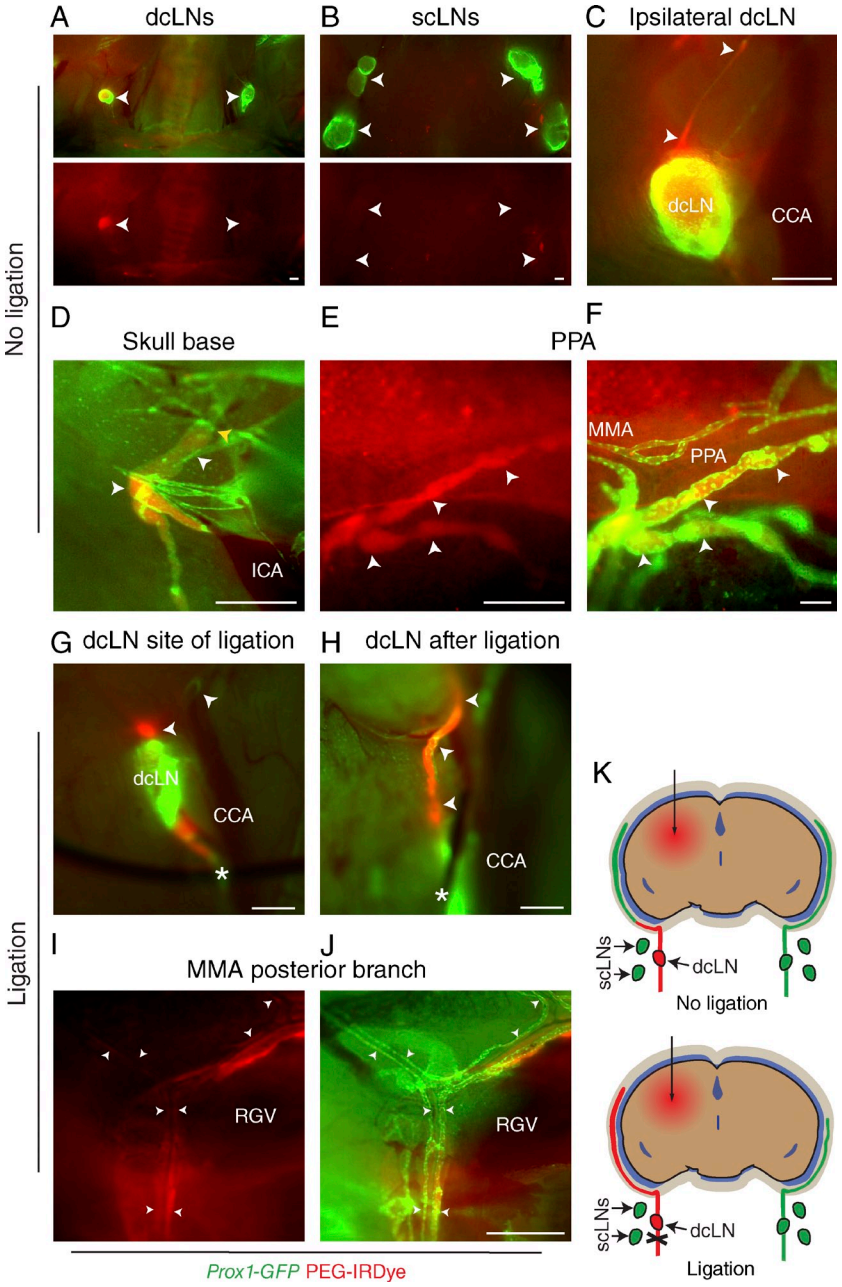

Figure 2. Dura mater lymphatic vessels drain brain ISF into dcLNs. (A–J) Analysis of lymphatic outflow routes of cerebral ISF by fluorescent stereomicroscopy in *Prox1-GFP* (green) mice 1 h after PEG-IRDye (red) injection into the brain parenchyma without (A–F) and with (G–J) ligation of the efferent lymphatic vessel of the dcLN. See K for schematic illustration of the experimental setup and summary of the results with and without ligation. (A and B) dcLNs and scLNs (both indicated with arrowheads) showing preferential filling of the ipsilateral dcLN but no filling in the scLNs. (C) Drainage into the ipsilateral dcLN via the efferent carotid lymphatic vessels (arrowheads). CCA, common carotid artery. (D) Internal carotid artery (ICA) and adjacent lymphatic vessels (white arrowheads) immediately below the osseous skull, showing drainage from the skull (yellow arrowhead). (E and F) Lymphatic vessels around the pterygopalatine artery (PPA), showing tracer uptake by the dura mater lymphatic vessels (arrowheads) only in the basal parts of the skull, nearby their exit site. MMA, middle meningeal artery. (G) Placement of a suture around the efferent lymphatic vessel (asterisk) of the dcLN. Arrowheads, afferent lymphatic vessels. (H) Afferent lymphatic vessel of the dcLN after ligation (asterisk), showing bulging of the afferent vessels (arrowheads). (I and J) Lymphatic vessels around the posterior branch of the MMA, showing increased filling of lymphatic vessels after ligation, extending above the retroglenoid vein (RGV) level. $n = 2–3$/group. Data are representative of two independent experiments. Bars: (A–E and G–J) 500 µm; (F) 100 µm.

drainage of brain ISF was confirmed by visualization of an intense signal in the dcLN but not in the superficial cervical LNs (scLNs; Fig. 2, A and B). Preferential drainage into the dcLN ipsilateral to the side of injection was observed (Fig. 2, A and C). When the tracer-filled afferent lymphatic vessels of the dcLNs were followed upstream, the vessels appeared to drain from the base of the skull (Fig. 2, C and D). Inside the skull, some PEG-IRDye filling of dura mater lymphatic vessels was observed only in the basal parts of the skull (Fig. 2, E and F), suggesting uptake by the lymphatic vessels but a quick washout. When the efferent lymphatic vessel of the dcLN was ligated (Fig. 2, G and H), enhanced filling of the dural lymphatic vessels was observed (Fig. 2, I–K). These data suggest that the dura mater lymphatic vessels absorb brain ISF/CSF from the subarachnoid space for transport into downstream dcLNs.

Absence of dura mater lymphatic vasculature in K14–VEGFR3–Ig mice

VEGF-C/D signaling via VEGFR3 is a critical regulator of lymphangiogenesis (Secker and Harvey, 2015). To (a) study whether dura mater lymphatic vessels are regulated by VEGFC/D–VEGFR3 signaling and (b) characterize an animal model in which the functional consequences of dura mater lymphatic vessel aplasia can be examined, we investigated the *K14-VEGFR3-Ig* transgenic (TG) mouse, which has impaired

VEGF-C/D–VEGFR3 signaling. These mice express a soluble VEGF-C/D trap protein consisting of the ligand-binding Ig homology domains 1–3 of VEGFR3 fused with the Fc domain of Igγ (Mäkinen et al., 2001). Although the VEGF-C/D trap transgene is expressed in keratinocytes, the circulating protein inhibits lymphangiogenesis in most tissues, and the mice display LN hypoplasia (Mäkinen et al., 2001; Alitalo et al., 2013). Lymphatic vessels were absent from both superior and basal parts of the skull in the TG mice compared with WT littermate mice (Fig. 3, A–F). Surprisingly, the mice displayed absence of only the scLNs but not dcLNs (Fig. 3, G–I; and Fig. 4 C). These data indicate that the dura mater lymphatic vessels are very sensitive to the inhibition of VEGF-C/D signaling and that the *K14-VEGFR3-Ig* TG mouse is a suitable model for studying the functional consequences of the absence of lymphatic drainage from the brain.

Lack of dural lymphatic vessels compromises CNS macromolecule clearance

First, we hypothesized that the absence of dura mater lymphatic vessels would impair the clearance of ISF and solutes from the brain. Thus, brain water content and ISF pressures (IFPs) were measured in TG and WT mice. Surprisingly, the IFP (TG vs. WT: 2.50 ± 0.54 vs. 2.53 ± 0.53 mmHg, P = 0.92, *n* = 6/group) and water content (TG vs. WT: 3.68 ± 0.023 vs. 3.71 ± 0.043 g/g dry weight, P = 0.27, *n* = 4/group) were not significantly different between the two groups. These results suggest that in physiological conditions, the brain has alternative ways to manage fluid extravasated from the blood vessels.

Second, we hypothesized that the absence of dura mater lymphatic vessels may impair macromolecule clearance from the brain. To test this, we studied the cerebral clearance of Alexa Fluor 488–conjugated OVA (A488-OVA, ∼45 kD), a macromolecule which retains fluorescent signal during fixation. We recorded cerebral, dcLN, and dura mater lymphatic vessel fluorescence from tissues 2 h after injection into the brain parenchyma of TG and WT littermate mice. Mice were perfusion fixed after sacrifice to prevent outflow of the tracer. Interestingly, the TG mice displayed a significant reduction in the amount of OVA cleared at the 2-h time point after injection (Fig. 4, A and B). Furthermore, a nearly complete abrogation of OVA accumulation was observed in the dcLNs of the TG mice (Fig. 4, C and D). Tracer-filled lymphatic vessels could be observed around the pterygopalatine artery and middle meningeal artery of WT mice, but this was absent in the TG mice (Fig. 4, E and F). To assess other possible causes for the drainage defect, we analyzed glymphatic function and the dcLN capacity for drainage. To this extent, the TG mice did not display qualitative defects in glymphatic function, as indicated by detectable paravascular outflow of the tracer in the subendothelial and perivascular space (Fig. 4, G and H), or a significant reduction in the amount of draining lymphatic vessels in the dcLN (Fig. 4, I and J). We also studied PEG-IRDye transfer from the subarachnoid space into the dcLNs after cisterna magna injection, which was significantly

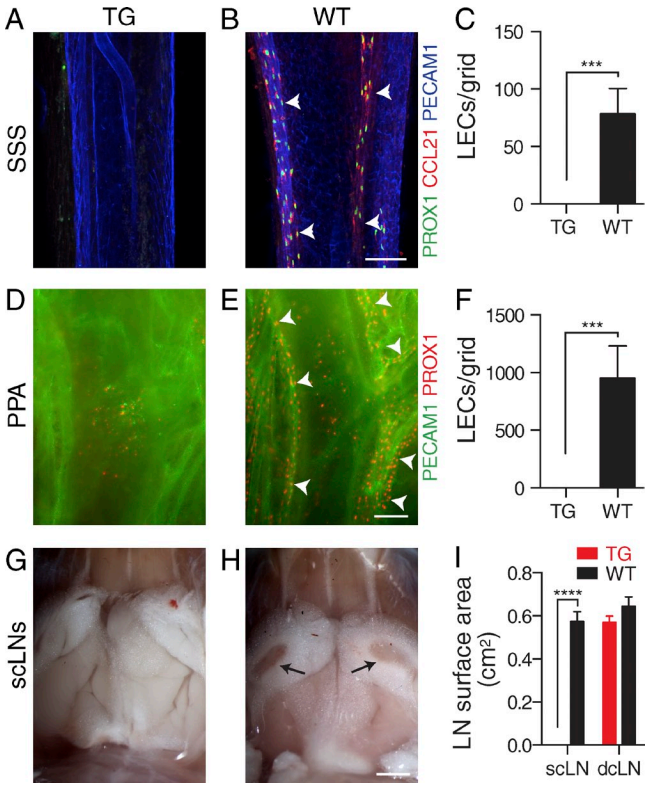

Figure 3. Absence of dural lymphatic vasculature in *K14-VEGFR3-Ig* TG mice. (A–F) Analysis of dura mater lymphatic vasculature in *K14-VEGFR3-Ig* TG and WT littermate control mice. (A–C) Immunofluorescence of the superior sagittal lymphatic vessels (arrowheads) for PECAM1, PROX1, and CCL21 (A and B) and quantification of PROX1⁺/CCL21⁺ lymphatic ECs (LECs)/grid (C). (D–F) Immunofluorescence of the pterygopalatine and middle meningeal lymphatic vessels (arrowheads) for PECAM1 and PROX1 (D and E) and quantification of PROX1⁺ LECs/grid (F). (G–I) Stereomicroscopic photographs showing the absence of the scLNs (arrows) in the TG mice (G and H) and quantification of the (mean left/right) scLN and dcLN surface areas (I). Micrographs of the dcLNs are shown in Fig. 4 C. (A–F) *n* = 3 (TG) and 4 (WT). (G and H) *n* = 4/group. Data are representative of two independent experiments. Bars: (A, B, D, and E) 100 µm; (G and H) 2 mm. Error bars indicate SD. Statistical analysis: two-tailed Student's *t* test (C and F) and two-way ANOVA followed by Šídák's post-hoc test (I). ***, P < 0.001; ****, P < 0.0001.

inhibited in the TG mice (Fig. 5). Overall, these data imply that the dura mater lymphatic vessels contribute to the clearance of macromolecules from the brain.

In this study, we report the surprising finding of a lymphatic vessel network in the dura mater of the CNS and show that dura mater lymphatic vessels are lined by fully differentiated PROX1⁺/VEGFR3⁺/LYVE1⁺/PDPN⁺/CCL21⁺/PECAM1^{low} lymphatic endothelium that is unique in its morphology and scarcity of valves. In the late eighteenth century the Italian anatomist Paolo Mascagni described what he called lymphatic vessels in the meninges and on the surface of the brain, but his finding could never be reproduced (Mascagni and Bellini, 1816; Lukić et al., 2003). The CNS proper has since been considered devoid of lymphatic vasculature.

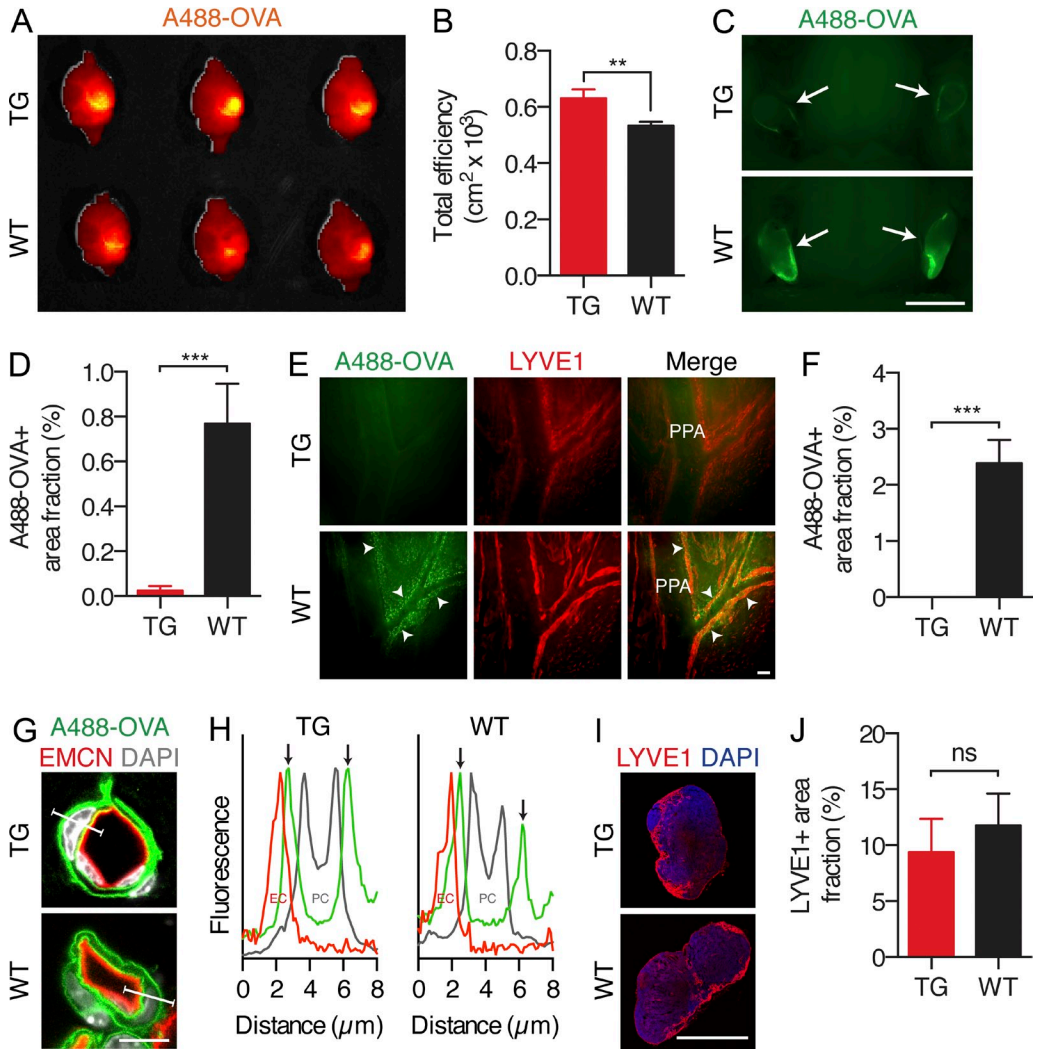

Figure 4. Lack of dural lymphatic vessels compromises CNS macromolecule clearance. Analysis of A488-OVA distribution 2 h after intraparenchymal injection in *K14-VEGFR3-Ig* TG mice and WT littermate controls. (A and B) Representative false color maps and quantification of the epifluorescence efficiency in the brain using IVIS imaging. (C and D) Representative images and quantification of the fluorescence in the dcLNs (indicated by arrows). (E and F) Representative fluorescent images of the A488-OVA tracer (indicated by arrowheads) accumulation in the LYVE1-stained lymphatic vessels around the PPA and MMA, with quantification of the A488-OVA–positive signal. Note the partial leakage of the tracer from the vessels caused by the perfusion fixation. (G) Fluorescent images of brain sections stained with DAPI and antibodies against endomucin (EMCN), showing the A488-OVA tracer distribution in the glymphatic system. (H) Plot profile analysis of the fluorescence along the indicated lines in G, showing A488-OVA signal in the subendothelial and perivascular spaces (arrows) in both TG and WT mice. (I) Immunofluorescent images of dcLNs stained with DAPI and antibodies against LYVE1. (J) Quantification of the LYVE1$^+$ area in the dcLNs in TG mice and WT littermate controls. (A, B, and G–J) $n = 4$ (TG) and 3 (WT). (C–F) $n = 3$ (TG) and 4 (WT). Data are representative of two independent experiments. Bars: (C) 2 mm; (E) 100 µm; (G) 8 µm; (I) 1,000 µm. Error bars indicate SD. Statistical analysis: two-tailed Student's *t* test. **, $P < 0.01$; ***, $P < 0.001$.

Incidentally, lymphatic vessels were mentioned in an electron microscopic study of the rat dura mater innervation. Furthermore, lymphatic vessels were detected in association with the murine cribriform plate and the human optic nerve (Andres et al., 1987; Gausas et al., 2007; Furukawa et al., 2008). However, the extent of the dura mater lymphatic network, or its role in CSF clearance, has not been realized.

According to the classical textbook model, CSF is produced by the choroid plexus, flows through the ventricles and the subarachnoid space, and is absorbed by arachnoid granulations for transport into the cerebral venous sinuses (Pollay, 2010). However, recent discoveries have established the glymphatic system as a critical regulator of cerebral waste clearance, especially during sleep (Iliff et al., 2012; Xie et al., 2013). In addition to the CSF clearance via arachnoid granulations, several studies have established that a part of brain ISF and CSF is drained into cervical LNs, yet it has been unclear how CSF enters the LNs (Koh et al., 2005; Weller et al., 2009). The observation of CSF tracers in the nasal lymphatic vessels under the cribriform plate has suggested clearance via olfactory

nerve sheaths through the cribriform plate (Kida et al., 1993; Koh et al., 2005). Additionally, CSF clearance has been observed to occur along spinal and cranial nerve sheaths with subsequent entry into extracranial lymphatic vessels (Miura et al., 1998; Weller et al., 2009).

Our data indicated filling of the dura mater lymphatic vessels after intraparenchymal injection of the tracer and the lack thereof in the *K14-VEGFR3-Ig* TG mice. This suggests a model in which a part of the brain ISF, downstream of the glymphatic system, is cleared directly from the subarachnoid space as CSF into the dura mater lymphatic vasculature. Interestingly, we also observed lymphatic vessels draining out of the skull along the dura mater of cranial nerves. Furthermore, we observed lymphatic vessels crossing the cribriform plate, which may explain some of the previous observations. Because of the lack of other known direct anatomical connections between the CSF space and extracranial lymphatic vessels, the dura mater lymphatic vessels are likely to represent the most important CSF source for the extracranial lymph compartment.

The importance of understanding the mechanisms of brain waste management are highlighted in patients suffering from Alzheimer's disease and other neurodegenerative diseases characterized by the pathological accumulation of misfolded proteins, such as amyloid β, into the brain parenchyma (Deane et al., 2008; Huang and Mucke, 2012). In other tissues, lymphatic vessels are critical for the absorption of macromolecules (Tammela and Alitalo, 2010). In the brain under physiological conditions, a major part of the cerebral amyloid β is removed by the transvascular route (Zlokovic, 2011; Zhao et al., 2015). However, recent evidence suggests that the glymphatic system may also be key in amyloid β clearance (Iliff et al., 2012). The present data show that the absence of dura mater lymphatic drainage results in inhibited clearance of OVA from the brain interstitium, suggesting that dura mater lymphatic vessels are critical for the absorption of macromolecules from the brain ISF and CSF.

Importantly, these findings open new avenues for research. Several other potential roles of dura mater lymphatic vessels can be envisioned, such as in the trafficking of cerebral immune cells, in antigen presentation in the dcLNs, and in the clearance of brain edema. These data may also explain why primary brain tumors can rarely metastasize into cervical LNs (Mondin et al., 2010). Interestingly, surgical removal of the dcLN results in cognitive impairment in mice (Radjavi et al., 2014), and ligation of the deep cervical lymphatic vessels has been reported to aggravate cerebral ischemia after stroke by increasing brain water edema and infarction volume in rats (Si et al., 2006). Further studies should be conducted to define the full contribution of dura mater lymphatic vasculature in CNS homeostasis and disease.

MATERIALS AND METHODS

Study approval. The study was approved by the Committee for Animal Experiments of the District of Southern Finland.

Mice and tissues. The *K14-VEGFR3$_{1-3}$-Ig* (FVB/N and C57BL/6J backgrounds; Mäkinen et al., 2001), *Prox1-GFP* (C57BL/6J albino background; Choi et al., 2011), and *Vegfr3$^{+/LacZ}$* (FVB/N background; Dumont et al., 1998) mouse lines have been published previously. WT littermate mice were used as controls. For WT analysis, C57BL/6J mice were used. For tissue analysis, mice were given a lethal dose of ketamine and xylazine and perfusion fixed through the left ventricle with ice-cold 1% paraformaldehyde (PFA) after puncture of the right auricle. The tissues were immediately immersed in 4% ice-cold PFA and postfixed overnight at 4°C, washed in PBS, and processed for staining. *Prox1-GFP* mouse tissues were freshly imaged without fixation.

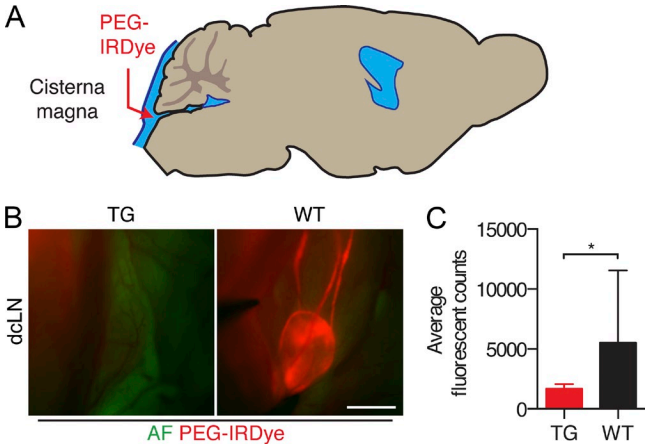

Figure 5. Lack of dural lymphatic vasculature inhibits CSF uptake into the dcLNs. (A) Schematic illustration of the experimental setup. (B) Representative fluorescent images of the dcLN in TG and WT mice 30 min after PEG-IRDye injection into the cisterna magna. AF, green channel autofluorescence. Bar, 1,000 µm. (C) Quantification of the dcLN fluorescence. $n = 6$ (TG) and 5 (WT). Data are representative of two independent experiments. Error bars indicate SD. Statistical analysis: two-tailed Student's t test. *, $P < 0.05$.

Immunostaining and X-gal staining. For whole-mount staining of the skull bones for laser-scanning confocal microscopy, the fixed skulls were dissected and underwent a mild decalcification with 0.5 M EDTA, pH 7.4, overnight at 4°C. For whole-mount staining of the basal skull for fluorescent stereomicroscopy, no decalcification was performed. After washes with PBS, the tissues were permeabilized in 0.3% Triton X-100 in PBS (PBS-TX) and blocked in 5% donkey serum/2% bovine serum albumin/0.3% PBS-TX. Primary antibodies were added to the blocking buffer and incubated with the tissue overnight at room temperature (RT). After washes in PBS-TX, the tissues were incubated with fluorophore-conjugated secondary antibodies in PBS-TX overnight at RT, followed by washing in PBS-TX. After postfixation in 1% PFA, the superior portions of the skull were washed with PBS and mounted in Mowiol 4-88 mounting medium (Sigma-Aldrich) containing 1,4-diazabicyclo[2.2.2]octane (DABCO; Sigma-Aldrich) and sealed with Cytoseal (Thermo Fisher Scientific). Clothespins were used to hold the coverslip and the microscopic slide together before the Cytoseal and Mowiol hardened. Tissues for fluorescent stereomicroscopy were stored in PBS and imaged immediately.

For cryosections of the skull, the fixed tissues underwent decalcification with 0.5 M EDTA, pH 7.4, for 72 h, immersion into 20% sucrose and 2% polyvinylpyrrolidone (PVP) for 24 h at 4°C, embedding in OCT compound (Tissue-Tek), and freezing for storage at −80°C. For other cryosections, the fixed tissues were immersed into 25% sucrose and embedded as above. Tissues were cut into 10–100-µm sections using a cryostat (Microm HM 550; Thermo Fisher Scientific). The sections were air-dried, encircled with a pap-pen, rehydrated in PBS, and blocked with 3% BSA in PBS-TX at RT. After primary antibody incubation at 4°C in 3% BSA in PBS overnight, the sections were washed with PBS and incubated for 2–3 h with the appropriate fluorophore-conjugated secondary antibody conjugates and 3% BSA in PBS. After washes with 0.1% PBS-TX, the sections were mounted with

Vectashield mounting medium containing DAPI (Vector Laboratories). For X-gal staining of skulls from *LacZ* reporter mice, the tissues were fixed with 0.2% glutaraldehyde and stained by the β-galactosidase substrate X-Gal (Promega) with a published protocol (Karkkainen et al., 2004).

Blood vessel labeling with DiI. Blood vessels of *Prox1-GFP* mice were labeled by cardiac perfusion using a fluorescent lipophilic carbocyanine dye DiI as previously described (Li et al., 2008). DiI incorporated into the EC membranes was visualized with fluorescent stereomicroscopy.

Antibodies. The following primary antibodies were used for immunostaining of mouse tissues: rabbit anti–mouse PROX1 (1:200; Petrova et al., 2008), goat anti–human PROX1 (1:500; R&D Systems), polyclonal goat anti–mouse VEGFR3 (1:50; R&D Systems), rat anti–mouse PECAM-1 (1:500; clone MEC 13.3; BD), polyclonal rabbit anti–mouse LYVE1 (1:1,000; Karkkainen et al., 2004), goat anti-CCL21 (1:500; R&D Systems), IgG fraction of rabbit polyclonal anti–mouse PDPN (1:500; provided by D. Kerjaschki, University of Vienna, Vienna, Austria; Wick et al., 2007), and rat anti–mouse endomucin (EMCN; 1:500; clone V.7C7; Santa Cruz Biotechnology, Inc.). The primary antibodies were detected with the appropriate Alexa Fluor 488, 568/594, or 633/647 secondary antibody conjugates (1:500; Molecular Probes/Invitrogen).

Intraparenchymal PEG-IRDye and A488-OVA clearance. To evaluate the outflow pathways and clearance of tracers from the brain interstitium, mice were anesthetized with a mixture of 80 mg/kg ketamine (Ketalar; Pfizer) and 6 mg/kg xylazine (Rompun vet; KVP Pharma + Veterinär Produke GmbH) or 160 mg/kg ketamine (Narketan; Vétoquinol) and 0.4 mg/kg medetomidine (Domitor; Orion Pharma) and placed into a stereotactic device. A midline skin incision was made to reveal the skull bone, which was thinned with a dental drill ∼2 mm lateral and 2.5 mm caudal to the bregma. 4 mg/ml A488-OVA (O-34781; Molecular Probes) or 20 µM of 20-kD PEG-IRDye (provided by P. Luciani and J.-C. Leroux, ETH Zurich, Zurich, Switzerland; Proulx et al., 2013) was injected into a 2-mm depth from the bregma in 0.5 µl with a 34-G Hamilton needle at a 0.1 µl/min rate over 5 min with a syringe pump (Harvard Apparatus). After the indicated time, the mice were sacrificed with a lethal dose of anesthesia. For visualization of PEG-IRDye, tissues were immediately imaged ex vivo. For visualization of A488-OVA, mice were perfusion fixed, and the entire head and neck with the cervical LNs were immersed in 4% ice-cold PFA and further postfixed overnight at 4°C with constant shaking. Fixed tissues were then washed in PBS and processed for imaging or staining as described above.

Cisterna magna PEG-IRDye clearance. To evaluate the PEG-IRDye clearance from the subarachnoid space, mice were anesthetized with a mixture of 160 mg/kg ketamine (Narketan) and 0.4 mg/kg medetomidine (Domitor) and placed into a stereotactic frame. The neck muscles were bluntly dissected through a small midline incision to reveal the dura mater overlying the cisterna magna. 20 µM of 20-kD PEG-IRDye was injected into the subarachnoid space in 10 µl with a 34-G Hamilton needle at a rate of 2 µl/min over 5 min with a syringe pump.

Image acquisition, processing, and quantitative analysis. Laser-scanning confocal micrographs of the fluorescently labeled samples were acquired at high resolution with an LSM 780 microscope (Carl Zeiss; air objectives 10× Plan-Apochromat with NA 0.45 and 20× Plan-Apochromat with NA 0.80, oil objective 40× Plan-Neofluar with NA 1.3 and oil objective 63× Plan-Apochromat with NA 1.4) using multichannel scanning in frame. The ZEN 2010 software (Carl Zeiss) was used for image acquisition.

Fluorescent stereomicrographs of labeled samples were obtained with an Axio Zoom.V16 fluorescence stereo zoom microscope (Carl Zeiss) equipped with an ORCA-Flash 4.0 digital sCMOS camera (Hamamatsu Photonics) or an OptiMOS sCMOS camera (QImaging). The ZEN 2012 software (Carl Zeiss) was used for image acquisition. Brain epifluorescence images were obtained with a Caliper IVIS Kinetic imaging system (PerkinElmer) equipped with a XFO-6 (Dolan-Jenner Fiber-Lite PL-900 Illuminator; quartz halogen lamp) for fluorescent imaging and an iXon$^+$ 888 EMCCD camera (Andor Technology). Images were processed and region of interest efficiencies were calculated with the Living Image 3.2 software. Image brightness and contrast were adjusted using ImageJ (National Institutes of Health) or Photoshop (Adobe) software. Quantitative analysis of the micrographs was performed using the ImageJ software.

Measurement of brain water content. Mice were sacrificed with carbon dioxide. The brains were removed from the skull and placed on a preweighed piece of aluminum foil and immediately weighed to obtain the wet weight. The dry weight was recorded after dehydration for 5 d in an 80°C oven. Water content was calculated as (wet weight − dry weight)/dry weight. The data shown in the text is representative of two independent experiments.

Measurement of brain IFP. Mice were anesthetized with a mixture of 120 mg/kg ketamine (Ketalar) and 0.24 mg/kg medetomidine (Domitor) in saline given s.c. and placed into a stereotactic device. Using a dental drill (2 mm OD), the skull bone was thinned at a site 2 mm caudal and lateral to the bregma. Brain ISF pressure was measured with micropipettes, tip diameter 2–4 µm, as described in detail previously (Wiig and Reed, 1983). Pipettes were inserted through an intact dura, and pressures were recorded 150–300 µm into brain tissue. The data shown in the text is representative of three independent experiments.

Statistical analysis. All values are expressed as mean ± SD. Quantitative data were compared between different groups by two-sample (unpaired Student's) two-tailed *t* test assuming equal variance. Two-way ANOVA followed by Šídák's post-hoc test was used for multiple comparisons. Differences were considered statistically significant at $P < 0.05$.

Online supplemental material. Video 1 shows dura mater lymphatic vessels in the lateral aspects of the interior portions of the skull in sagittal plane in the *Prox1-GFP* mouse. Online supplemental material is available at http://www.jem.org/cgi/content/full/jem.20142290/DC1.

We thank Drs. Paola Luciani and Jean-Christophe Leroux for the PEG-IRDye; Dr. Dontscho Kerjaschki for the antibodies against PDPN; Kirsi Lintula, Riitta Kauppinen, Jarmo Koponen, and Tapio Tainola (University of Helsinki, Helsinki, Finland) for technical assistance; the Biomedicum Imaging Unit for help with imaging; and the staff of the University of Helsinki Laboratory Animal Centre for technical assistance with the mouse work.

This study was supported by grants from the Academy of Finland, the Sigrid Juselius Foundation, the European Research Council (ERC-2010-AdG-268804), the Swiss National Science Foundation (310030B_147087), VESSEL-Marie Curie multipartner Initial Training Network for Vascular Biology (EU FP7-PEOPLE-2012-ITN), the Leducq Transatlantic Network of Excellence on Lymph Vessels in Obesity and Cardiovascular Disease (11CVD03; to K. Alitalo and M. Detmar), and the Research Council of Norway (222278/F20).

The authors declare no competing financial interests.

Submitted: 8 December 2014
Accepted: 4 June 2015

REFERENCES

Alitalo, A.K., S.T. Proulx, S. Karaman, D. Aebischer, S. Martino, M. Jost, N. Schneider, M. Bry, and M. Detmar. 2013. VEGF-C and VEGF-D blockade inhibits inflammatory skin carcinogenesis. *Cancer Res.* 73:4212–4221. http://dx.doi.org/10.1158/0008-5472.CAN-12-4539

Andres, K.H., M. von Düring, K. Muszynski, and R.F. Schmidt. 1987. Nerve fibres and their terminals of the dura mater encephali of the rat. *Anat. Embryol. (Berl.).* 175:289–301. http://dx.doi.org/10.1007/BF00309843

Aspelund, A., T. Tammela, S. Antila, H. Nurmi, V.-M. Leppänen, G. Zarkada, L. Stanczuk, M. Francois, T. Mäkinen, P. Saharinen, et al. 2014. The Schlemm's canal is a VEGF-C/VEGFR-3-responsive lymphatic-like vessel. *J. Clin. Invest.* 124:3975–3986. http://dx.doi.org/10.1172/JCI75395

Choi, I., H.K. Chung, S. Ramu, H.N. Lee, K.E. Kim, S. Lee, J. Yoo, D. Choi, Y.S. Lee, B. Aguilar, and Y.-K. Hong. 2011. Visualization of lymphatic vessels by Prox1-promoter directed GFP reporter in a bacterial artificial chromosome-based transgenic mouse. *Blood*. 117:362–365. http://dx.doi.org/10.1182/blood-2010-07-298562

Deane, R., A. Sagare, and B.V. Zlokovic. 2008. The role of the cell surface LRP and soluble LRP in blood-brain barrier Aβ clearance in Alzheimer's disease. *Curr. Pharm. Des.* 14:1601–1605. http://dx.doi.org/10.2174/138161208784705487

Dumont, D.J., L. Jussila, J. Taipale, A. Lymboussaki, T. Mustonen, K. Pajusola, M. Breitman, and K. Alitalo. 1998. Cardiovascular failure in mouse embryos deficient in VEGF receptor-3. *Science*. 282:946–949. http://dx.doi.org/10.1126/science.282.5390.946

Furukawa, M., H. Shimoda, T. Kajiwara, S. Kato, and S. Yanagisawa. 2008. Topographic study on nerve-associated lymphatic vessels in the murine craniofacial region by immunohistochemistry and electron microscopy. *Biomed. Res.* 29:289–296. http://dx.doi.org/10.2220/biomedres.29.289

Gausas, R.E., T. Daly, and F. Fogt. 2007. D2-40 expression demonstrates lymphatic vessel characteristics in the dural portion of the optic nerve sheath. *Ophthal. Plast. Reconstr. Surg.* 23:32–36. http://dx.doi.org/10.1097/01.iop.0000249431.04116.a8

Hong, Y.-K., N. Harvey, Y.-H. Noh, V. Schacht, S. Hirakawa, M. Detmar, and G. Oliver. 2002. Prox1 is a master control gene in the program specifying lymphatic endothelial cell fate. *Dev. Dyn.* 225:351–357. http://dx.doi.org/10.1002/dvdy.10163

Huang, Y., and L. Mucke. 2012. Alzheimer mechanisms and therapeutic strategies. *Cell*. 148:1204–1222. http://dx.doi.org/10.1016/j.cell.2012.02.040

Iliff, J.J., and M. Nedergaard. 2013. The microcirculation—fantastic voyage: Is there a cerebral lymphatic system? *Stroke*. 44:S93–S95. http://dx.doi.org/10.1161/STROKEAHA.112.678698

Iliff, J.J., M. Wang, Y. Liao, B.A. Plogg, W. Peng, G.A. Gundersen, H. Benveniste, G.E. Vates, R. Deane, S.A. Goldman, et al. 2012. A paravascular pathway facilitates CSF flow through the brain parenchyma and the clearance of interstitial solutes, including amyloid β. *Sci. Transl. Med.* 4:147ra111. http://dx.doi.org/10.1126/scitranslmed.3003748

Karkkainen, M.J., P. Haiko, K. Sainio, J. Partanen, J. Taipale, T.V. Petrova, M. Jeltsch, D.G. Jackson, M. Talikka, H. Rauvala, et al. 2004. Vascular endothelial growth factor C is required for sprouting of the first lymphatic vessels from embryonic veins. *Nat. Immunol.* 5:74–80. http://dx.doi.org/10.1038/ni1013

Kida, S., A. Pantazis, and R.O. Weller. 1993. CSF drains directly from the subarachnoid space into nasal lymphatics in the rat. Anatomy, histology and immunological significance. *Neuropathol. Appl. Neurobiol.* 19:480–488. http://dx.doi.org/10.1111/j.1365-2990.1993.tb00476.x

Koh, L., A. Zakharov, and M. Johnston. 2005. Integration of the subarachnoid space and lymphatics: is it time to embrace a new concept of cerebrospinal fluid absorption? *Cerebrospinal Fluid Res.* 2:6. http://dx.doi.org/10.1186/1743-8454-2-6

Li, Y., Y. Song, L. Zhao, G. Gaidosh, A.M. Laties, and R. Wen. 2008. Direct labeling and visualization of blood vessels with lipophilic carbocyanine dye DiI. *Nat. Protoc.* 3:1703–1708. http://dx.doi.org/10.1038/nprot.2008.172

Liao, S., and P.Y. von der Weid. 2015. Lymphatic system: An active pathway for immune protection. *Semin. Cell Dev. Biol.* 38:83–89. http://dx.doi.org/10.1016/j.semcdb.2014.11.012

Lukić, I.K., V. Gluncić, G. Ivkić, M. Hubenstorf, and A. Marusić. 2003. Virtual dissection: a lesson from the 18th century. *Lancet*. 362:2110–2113. http://dx.doi.org/10.1016/S0140-6736(03)15114-8

Mäkinen, T., L. Jussila, T. Veikkola, T. Karpanen, M.I. Kettunen, K.J. Pulkkanen, R. Kauppinen, D.G. Jackson, H. Kubo, S. Nishikawa, et al. 2001. Inhibition of lymphangiogenesis with resulting lymphedema in transgenic mice expressing soluble VEGF receptor-3. *Nat. Med.* 7:199–205. http://dx.doi.org/10.1038/84651

Mascagni, P., and G.B. Bellini. 1816. Istoria Completa Dei Vasi Linfatici. Vol. II. Presso Eusebio Pacini e Figlio, Florence. 195 pp.

Miura, M., S. Kato, and M. von Lüdinghausen. 1998. Lymphatic drainage of the cerebrospinal fluid from monkey spinal meninges with special reference to the distribution of the epidural lymphatics. *Arch. Histol. Cytol.* 61:277–286. http://dx.doi.org/10.1679/aohc.61.277

Mondin, V., A. Ferlito, K.O. Devaney, J.A. Woolgar, and A. Rinaldo. 2010. A survey of metastatic central nervous system tumors to cervical lymph nodes. *Eur. Arch. Otorhinolaryngol.* 267:1657–1666. http://dx.doi.org/10.1007/s00405-010-1357-1

Oliver, G., and R.S. Srinivasan. 2010. Endothelial cell plasticity: how to become and remain a lymphatic endothelial cell. *Development*. 137:363–372. http://dx.doi.org/10.1242/dev.035360

Petrova, T.V., A. Nykänen, C. Norrmén, K.I. Ivanov, L.C. Andersson, C. Haglund, P. Puolakkainen, F. Wempe, H. von Melchner, G. Gradwohl, et al. 2008. Transcription factor PROX1 induces colon cancer progression by promoting the transition from benign to highly dysplastic phenotype. *Cancer Cell*. 13:407–419. http://dx.doi.org/10.1016/j.ccr.2008.02.020

Plog, B.A., M.L. Dashnaw, E. Hitomi, W. Peng, Y. Liao, N. Lou, R. Deane, and M. Nedergaard. 2015. Biomarkers of traumatic injury are transported from brain to blood via the glymphatic system. *J. Neurosci.* 35:518–526. http://dx.doi.org/10.1523/JNEUROSCI.3742-14.2015

Pollay, M. 2010. The function and structure of the cerebrospinal fluid outflow system. *Cerebrospinal Fluid Res.* 7:9. http://dx.doi.org/10.1186/1743-8454-7-9

Proulx, S.T., P. Luciani, A. Christiansen, S. Karaman, K.S. Blum, M. Rinderknecht, J.-C. Leroux, and M. Detmar. 2013. Use of a PEG-conjugated bright near-infrared dye for functional imaging of rerouting of tumor lymphatic drainage after sentinel lymph node metastasis. *Biomaterials*. 34:5128–5137. http://dx.doi.org/10.1016/j.biomaterials.2013.03.034

Radjavi, A., I. Smirnov, N. Derecki, and J. Kipnis. 2014. Dynamics of the meningeal $CD4^+$ T-cell repertoire are defined by the cervical lymph nodes and facilitate cognitive task performance in mice. *Mol. Psychiatry*. 19:531–532. http://dx.doi.org/10.1038/mp.2013.79

Secker, G.A., and N.L. Harvey. 2015. VEGFR signaling during lymphatic vascular development: From progenitor cells to functional vessels. *Dev. Dyn.* 244:323–331. http://dx.doi.org/10.1002/dvdy.24227

Si, J., L. Chen, and Z. Xia. 2006. Effects of cervical-lymphatic blockade on brain edema and infarction volume in cerebral ischemic rats. *Chin. J. Physiol.* 49:258–265.

Tammela, T., and K. Alitalo. 2010. Lymphangiogenesis: Molecular mechanisms and future promise. *Cell*. 140:460–476. http://dx.doi.org/10.1016/j.cell.2010.01.045

Weller, R.O., E. Djuanda, H.-Y. Yow, and R.O. Carare. 2009. Lymphatic drainage of the brain and the pathophysiology of neurological disease. *Acta Neuropathol.* 117:1–14. http://dx.doi.org/10.1007/s00401-008-0457-0

Wick, N., P. Saharinen, J. Saharinen, E. Gurnhofer, C.W. Steiner, I. Raab, D. Stokic, P. Giovanoli, S. Buchsbaum, A. Burchard, et al. 2007. Transcriptomal comparison of human dermal lymphatic endothelial cells ex vivo and in vitro. *Physiol. Genomics*. 28:179–192. http://dx.doi.org/10.1152/physiolgenomics.00037.2006

Wiig, H., and R.K. Reed. 1983. Rat brain interstitial fluid pressure measured with micropipettes. *Am. J. Physiol.* 244:H239–H246.

Xie, L., H. Kang, Q. Xu, M.J. Chen, Y. Liao, M. Thiyagarajan, J. O'Donnell, D.J. Christensen, C. Nicholson, J.J. Iliff, et al. 2013. Sleep drives metabolite clearance from the adult brain. *Science*. 342:373–377. http://dx.doi.org/10.1126/science.1241224

Zhao, Z., A.P. Sagare, Q. Ma, M.R. Halliday, P. Kong, K. Kisler, E.A. Winkler, A. Ramanathan, T. Kanekiyo, G. Bu, et al. 2015. Central role for PICALM in amyloid-β blood-brain barrier transcytosis and clearance. *Nat. Neurosci.* http://dx.doi.org/10.1038/nn.4025

Zlokovic, B.V. 2011. Neurovascular pathways to neurodegeneration in Alzheimer's disease and other disorders. *Nat. Rev. Neurosci.* 12:723–738. http://dx.doi.org/10.1038/mrm3114